cosmetics

MDPI

Article

Anti-Particulate Adhesion Efficacy of a Cosmetic Product: A Controlled In Vivo Study Using a Patented Exposure Chamber

Youngrin Kwag [1,2], Huijeong Jeong [1], Yoori Kang [1], Min Sook Jung [1], Wonkyu Hong [1,3,*] and Hongseok Kim [1,4,*]

[1] Human Skin Clinical Trial Center Co., Ltd., 62 Digital-ro 31-gil, Guro-gu, Seoul 08390, Republic of Korea; 2loveletter2@hanmail.net (Y.K.); skin@humantest.co.kr (H.J.); kyr@humantest.co.kr (Y.K.); msjung5481@gmail.com (M.S.J.)
[2] Department of Occupational and Environmental Medicine, School of Medicine, Ewha Womans University, Seoul 07804, Republic of Korea
[3] Class One Clinic, 10F Mijin Plaza, 390 Gangnam-daero, Gangnam-gu, Seoul 06232, Republic of Korea
[4] VOS Dermatology Clinic, 1–4F, 806 Eonju-ro, Gangnam-gu, Seoul 06022, Republic of Korea
* Correspondence: hwk0417@gmail.com (W.H.); drhong3@gmail.com (H.K.); Tel.: +82-70-5222-9663 (H.K.)

Abstract

This study validated a controlled in vivo test protocol using a patented particulate exposure chamber (Korean Patent No. 10-2020-0068941) to evaluate the anti-particulate adhesion efficacy of a cosmetic sunscreen formulation (SPF 50+, PA++++). The primary aim was methodological—to demonstrate that the chamber system can reliably detect differences in carbon black adhesion under standardised conditions. A split-site paired design was applied to 22 healthy adult females (mean age 60.3 ± 5.2 years; range 46–68 years). Carbon black particles (≤10 µm) were dispersed via a precision dual-stage pneumatic nozzle within a sealed chamber (22 ± 2 °C; 50 ± 5% RH). Between-group comparison was assessed by the Wilcoxon signed-rank test (primary) and the generalised estimating equation (GEE) model (complementary between-group comparison per institutional SOP). The treated site showed a 55.0% reduction in carbon black adhesion (treated: 4243 ± 2225 pixels; control: 9430 ± 4769 pixels, SE = 4.82, 95% CI: −64.4 to −45.6, Wald Z = −11.41, $p < 0.001$; Cohen's d = 2.43). The Wilcoxon test confirmed the result independently (Z = −4.11, $p < 0.001$). All 22 subjects (100%) showed consistent reduction directionality (individual rates: 22.6–74.2%; mean 51.8%; median 52.3%). Bootstrap resampling (n = 10,000), outlier-exclusion, and exact sign test sensitivity analyses all confirmed robustness. These findings represent proof-of-concept methodological validation applied to a single product under accelerated exposure conditions.

Keywords: anti-particulate adhesion; claim substantiation; controlled exposure chamber; particulate matter; skin physiology; carbon black

Check for updates

Academic Editors: Piergiacomo Calzavara-Pinton and Simone Soglia

Received: 9 May 2026
Revised: 30 May 2026
Accepted: 17 June 2026
Published: 19 June 2026

Copyright: © 2026 by the authors. Licensee MDPI, Basel, Switzerland. This article is an open access article distributed under the terms and conditions of the Creative Commons Attribution (CC BY) license.

1. Introduction

The progressive industrialisation and urbanisation of modern society have led to a sustained increase in atmospheric particulate matter (PM) concentrations. Airborne PM is now recognised as a major environmental hazard that adversely affects not only the respiratory system but also skin health [1–4]. PM deposited on the skin surface can occlude pores and trigger oxidative stress, promoting the generation of reactive oxygen species (ROS) that impair skin barrier function, increase inflammatory cytokine secretion,

and accelerate skin ageing [5–9]. In particular, particles with a diameter of 10 μm or less (PM10) and 2.5 μm or less (PM2.5) can penetrate the skin via hair follicles and sweat glands, raising further concern about their potential for harm [10–13]. Mechanistically, PM activates cellular signalling pathways—including the aryl hydrocarbon receptor (AhR), NF-κB, and MAPK cascades—amplifying oxidative stress and inflammatory cytokine production [14]. PM exposure also disrupts the skin microbiome, reducing microbial diversity and further compromising barrier integrity [15].

Against this background, the cosmetic industry has seen a rapid increase in demand for anti-pollution cosmetics capable of protecting the skin from particulate matter [14–16]. Epidemiological studies have repeatedly confirmed that exposure to air pollution is significantly associated with facial pigmentation, wrinkling, and accelerated skin ageing [17–19]. The primary protective mechanism by which cosmetics mitigate PM adhesion to the skin involves the formation of a continuous physical film on the skin surface. Film-forming polymers—including silicones, acrylate copolymers, and wax-based ingredients—create a smooth, hydrophobic barrier that reduces the electrostatic and van der Waals interactions between airborne particles and the skin [14,15]. Additionally, ingredients with high surface tension and occlusive properties limit PM penetration into follicular openings and intercellular spaces, thereby providing a complementary mechanical shield [16,20]. Despite this mechanistic rationale, the evidence base for anti-PM claim substantiation remains methodologically heterogeneous. Existing approaches range from in vitro tape-stripping coupled with ICP-MS [21] and ex vivo skin models [22] to open-enclosure in vivo challenge designs [23–25]. A critical limitation shared by many is insufficient environmental control—particularly of particle concentration, temperature, and humidity —which compromises reproducibility and inter-laboratory comparability [3,26,27].

Recognising the growing public health relevance of PM exposure, the Ministry of Food and Drug Safety (MFDS) of the Republic of Korea has published guidelines for the efficacy evaluation of cosmetics bearing anti-particulate matter claims, stipulating that substantiation should be based on scientifically appropriate in vivo or in vitro methods [28]. However, these guidelines do not prescribe a standardised chamber-based exposure protocol for in vivo testing, and leave the specific apparatus design, environmental control parameters, and particle dispersal methodology to the discretion of the testing laboratory. Whilst a recent review highlighted the breadth of efficacy testing approaches available for anti-pollution claim substantiation [29], these methods may have limitations in terms of ecological relevance and result consistency when environmental variables are insufficiently controlled [3,21–23].

To address these limitations, our institution has developed a patent-based chamber system that enables controlled exposure of human skin to fine particles (Korean Patent No. 10-2020-0068941). The device incorporates an environmental control system capable of precisely regulating temperature and relative humidity within a sealed chamber, and a dual-stage pneumatic nozzle comprising a primary low-pressure aerosolisation stage and a secondary high-pressure dispersion stage, designed to prevent particle agglomeration and ensure uniform particle distribution. Active air circulation throughout the chamber interior further approximates real-world atmospheric exposure conditions. Following each test session, an integrated automatic cleaning system—comprising a pre-filter, HEPA filter, and dust collector—purges residual particles from the chamber, preventing cross-contamination between successive test runs.

The present study aimed to validate this chamber-based in vivo protocol and demonstrate its application to evaluating a commercially available anti-pollution cosmetic. Using a split-site paired design within each participant's forearm [30], we assessed whether differences in carbon black adhesion could be reliably detected whilst minimising inter-

individual variability. The primary objective was platform validation rather than product characterisation; findings should therefore be interpreted as proof-of-concept evidence.

2. Materials and Methods

2.1. Test Product

The test product was a commercially available sunscreen formulation (SPF 50+, PA++++; IALL Co., Ltd., Seoul, Republic of Korea) marketed as having anti-pollution functionality. Per the sponsor's data confidentiality agreement, the full INCI list was not disclosed; however, the product's functional category (leave-on film-forming emulsion), primary mechanism (physical barrier formation via polymeric film), and physicochemical properties (viscosity: 8000–12,000 mPa·s; post-application film thickness: ~5–8 µm) were approved for disclosure by the manufacturer. The present study focused on validating the chamber-based evaluation platform; INCI non-disclosure does not therefore affect the validity of the efficacy measurements reported. Carbon black (mean particle size $\leq$ 10 µm; Sigma-Aldrich, St. Louis, MO, USA) served as the model test particle, widely employed in in vivo anti-PM adhesion evaluations [21,22]. The product was applied uniformly at 2 mg/cm^2 using a calibrated syringe.

2.2. Test Apparatus: Patented Particulate Exposure Chamber

The PM exposure system is the anti-dust performance testing device registered as Korean Patent No. 10-2020-0068941 (filing date: 8 June 2020). The apparatus is based on a sealed chamber completely isolated from the external environment. An operator access port is located at the upper portion for handling the spray nozzle and maintenance, whilst subject forearm insertion ports are situated at the lower portion. Compressed-air-sealed shielding tubes at each insertion port simultaneously prevent particle leakage to the exterior and ingress of ambient air during exposure.

Particle supply is achieved via a dual-stage pneumatic spray nozzle. Low-pressure compressed air supplied through the first inlet at the lower end aerosolises carbon black particles loaded in the vessel; subsequently, high-pressure compressed air supplied through the second inlet at the upper end disperses the aerosolised particles uniformly into the chamber. This precision dual-stage mechanism prevents particle agglomeration and ensures homogeneity of particle concentration, enabling reproducible exposure conditions across subjects.

The internal environment was maintained at 22 $\pm$ 2 °C and 50 $\pm$ 5% relative humidity by a temperature and humidity control system comprising a circulation fan, heater unit, temperature/humidity sensor, and central controller. Active air circulation drives continuous movement of aerosolised particles, creating a dynamic exposure environment that more faithfully replicates real-world atmospheric conditions compared with static, open-enclosure approaches. After testing, residual particles are automatically removed through a pre-filter, HEPA filter, and dust collector in the exhaust duct; this automated cleaning function eliminates cross-contamination between successive test runs and ensures operator safety. The overall configuration is presented in Figure 1. The carbon black mass concentration within the chamber during the 5 min exposure period was designed to approximate 200–3000 mg/m^3, corresponding to approximately 100–1500 times the ambient PM_{10} level, consistent with an accelerated challenge test paradigm. This accelerated paradigm was intentionally designed to compress the cumulative outdoor PM exposure typically experienced over 8–24 h into a 5 min-controlled laboratory session, enabling reliable between-site differentiation within a single participant visit. Precedent for accelerated PM challenge concentrations in cosmetic testing has been established [20,29]. The extent to which efficacy detected under these conditions translates to real-world protection warrants further investigation.



Figure 1. Schematic of the patented controlled particulate exposure chamber (Korean Patent No. 10-2020-0068941). (**A**) External view showing the upper operator access port, lower subject forearm insertion ports, control panel, and mobility casters. (**B**) Internal cross-section showing the central spray nozzle, air-circulation duct (heater, temperature/humidity sensor, fan), exhaust line (pre-filter, HEPA filter, dust collector), compressed-air supply lines, and central controller. (**C**) Dual-stage pneumatic nozzle mechanism: the lower first inlet (low-pressure) aerosolises carbon black within the vessel; the upper second inlet (high-pressure) disperses the aerosolised particles uniformly into the chamber.

2.3. Subjects

Twenty-two healthy adult females aged 46–68 years were enrolled. Sample size was determined a priori based on a two-sided paired comparison, assuming a mean group-level reduction rate of 50%, a standard deviation of 25 percentage points, a two-sided α of 0.05, and a statistical power of 80%, yielding a minimum required sample of 17 subjects; 22 subjects were enrolled to provide an additional statistical margin and to account for potential dropouts. Inclusion criteria were: (1) absence of skin disease or wounds at the bilateral volar forearm test sites; (2) no use of cosmetics or topical preparations at the test sites for at least two weeks before the study; (3) not pregnant or breastfeeding; and (4) willingness to provide voluntary written informed consent. The study was approved by the Institutional Review Board (IRB approval number: HM-IRB-P25-1115) and conducted in accordance with the Declaration of Helsinki. Written informed consent was obtained from each participant before enrolment. The test period was 19–20 January 2026; there were no withdrawals or adverse events.

2.4. Study Design and Procedure

A split-site paired design was used in which treated and control sites were compared within the same subject's forearm [24]. Two 3 × 3 cm sites on the volar forearm of each subject were randomly designated as treated (product-applied) or control (untreated). After a 30 min acclimatisation period (22 ± 2 °C, 50 ± 5% relative humidity), the test product was applied uniformly to the treated site only. Following a 15 min absorption period, both sites were inserted into the patented chamber, and carbon black was dispersed according to the standard protocol for 5 min. After exposure, subjects proceeded immediately to image acquisition. Image analysis was performed by an outcome assessor blinded to treatment allocation. The quantitative analysis relied on a pre-defined pixel-intensity threshold applied uniformly across all images, minimising subjective judgement in particle segmentation. The complete procedure is shown in Figure 2. Site allocation was determined by computer-generated block randomisation (block size = 2) performed by an independent statistician prior to enrolment; the allocation list was concealed until product application. Baseline skin hydration (Corneometer CM 825; Courage + Khazaka Electronic, Cologne, Germany) and sebum level Sebumeter SM 815; Courage + Khazaka Electronic, Cologne, Germany) were recorded at both sites to confirm between-site comparability. The study employed a single-blind design: participants were unaware of treatment allocation; image acquisition and analysis were performed by an operator blinded to site assignment. Procedural timing: acclimatisation T = 0–30 min; product application T = 30–45 min; chamber exposure T = 45–50 min; post-exposure imaging T = 50–80 min; cleaning verification T = 80–90 min.

2.5. Image Acquisition and Quantitative Analysis

Carbon black particles adhered to the skin surface were observed and quantified using a portable digital microscope (Dino-Lite Premier AM3113T; AnMo Electronics, New Taipei City, Taiwan). All images were captured at ×50 magnification with the microscope perpendicular to the skin at a fixed working distance of 3 cm; built-in polarised LED ring illumination was set to uniform intensity. Images were captured in a dedicated darkened room by the same trained operator. Images were analysed using Image-Pro 10 (Media Cybernetics, Rockville, MD, USA) with a standardised macro; a region of interest (ROI) of identical size was defined in each image, and particle segmentation was based on pixel-intensity contrast between skin surface and adhered particles. The relative reduction effect was calculated as image analysis validation: a calibration reference grid was imaged at the start of each session to ensure spatial consistency. Automated Otsu thresholding was applied uniformly across all images under identical white balance and illumination

settings, ensuring objective and consistent particle segmentation. As an indirect indicator of measurement consistency, the coefficients of variation (CVs) of post-exposure pixel area were 52.4% in the treated group and 50.6% in the control group; the near-identical CVs between groups indicate that inter-subject biological variability—rather than measurement inconsistency—is the primary source of variance.

$$\text{Reduction rate (\%)} = [(\text{Control pixel area} - \text{Treated pixel area})/\text{Control pixel area}] \times 100$$

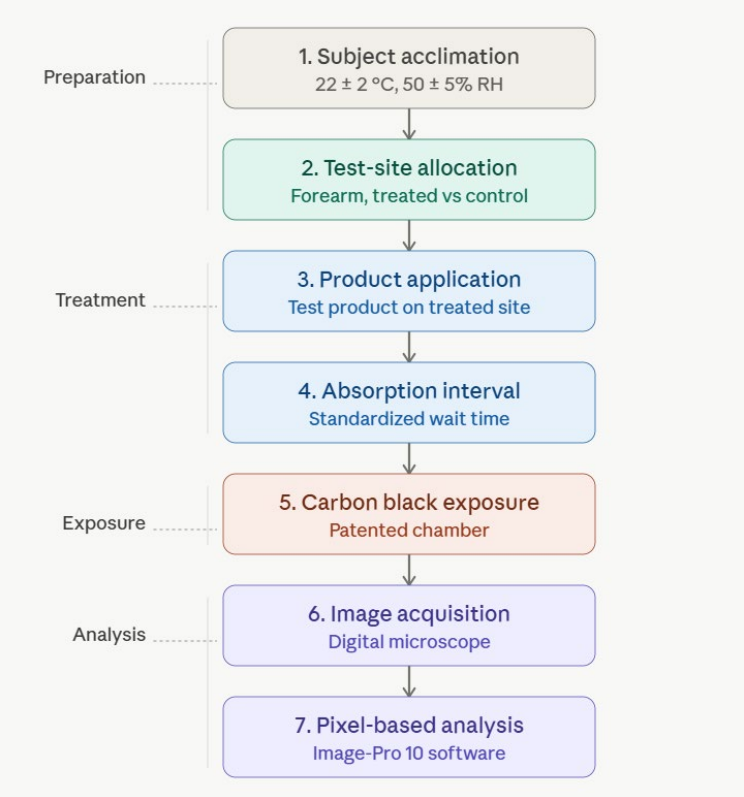


Figure 2. Standardised workflow of the in vivo anti-particulate adhesion test with procedural timing. The protocol comprises: subject acclimatisation (T = 0–30 min), test-site allocation and baseline biophysical measurement, product application and absorption (T = 30–45 min), carbon black chamber exposure (T = 45–50 min), digital microscopic image acquisition (T = 50–80 min), and cleaning verification (T = 80–90 min). Pixel-based quantitative analysis using Image-Pro 10.

2.6. Statistical Analysis

Demographic characteristics of the 22 study participants are summarised in Table 1. Data are presented as mean ± SD. Non-normality of post-exposure pixel area was confirmed by the Shapiro–Wilk test ($W = 0.89$, $p = 0.023$). Given confirmed non-normality, the Wilcoxon signed-rank test was applied as the primary analysis on within-subject differences (control minus treated pixel area). As a complementary between-group comparison consistent with institutional SOP for non-normal data [31–33], Robust sandwich standard errors were applied. Full GEE output (β, SE, 95% CI, Wald Z, working correlation ρ) is reported in Table 2. Effect size was quantified as Cohen's d on within-subject differences. Additionally, bootstrap resampling ($n = 10{,}000$) was conducted to derive bootstrap 95% CIs, and an exact binomial sign test was applied to assess the probability of 100% directional consistency under the null hypothesis. An outlier-excluded sensitivity analysis removed subjects with individual reduction rates outside ±2 SD of the mean. All analyses were performed in SPSS v26.0 (IBM Corp., Armonk, NY, USA). Full individual-level data and extended sensitivity analyses are provided in the Supplementary Materials.

Table 1. Demographic characteristics of the study subjects (n = 22).

Characteristic	Value
Sex	Female, 22 (100%)
Age, mean ± SD (years)	60.27 ± 5.21
Age range (years)	46–68
Withdrawals	0
Adverse events	None reported

SD, standard deviation.

Table 2. Carbon black adhesion area in treated and control sites before and after chamber exposure.

Assessment	Treated Site (Pixels)	Control Site (Pixels)	*p*-Value
Baseline	0.00 ± 0.00	0.00 ± 0.00	—
Post-exposure	4243.27 ± 2224.84	9430.32 ± 4769.35	<0.001
Mean reduction (%)	55.0%	—	—
GEE β (pp, complementary)	−55.0	—	—
SE	4.82	—	—
95% CI (pp)	−64.4 to −45.6	—	—
Wald Z	−11.41	—	—
p-value	<0.001	—	—
Working correlation ρ	0.63 (exchangeable)	—	—
Cohen's d	2.43 (large)	—	—
Wilcoxon Z/p	−4.11/<0.001	—	—

Values are mean ± SD unless otherwise stated. GEE: exchangeable working correlation (ρ = 0.63); robust sandwich standard errors (complementary between-group analysis). pp = percentage points. Cohen's d = 2.43 (large effect). Wilcoxon signed-rank: Z = −4.11, $p < 0.001$. Image analysis: Image-Pro 10 (Media Cybernetics). SD, standard deviation; CI, confidence interval.

3. Results

3.1. Demographic Characteristics

All 22 subjects were female with a mean age of 60.27 ± 5.21 years (range 46–68 years). There were no withdrawals, and no adverse events were reported. Subject characteristics are summarised in Table 1.

3.2. Comparison of Carbon Black Adhesion Between Treated and Control Sites

At baseline, pixel areas were zero in both groups, confirming the absence of residual particles at test commencement. After exposure, the mean pixel area was 4243.27 ± 2224.84 pixels in the treated group and 9430.32 ± 4769.35 pixels in the control group. The Wilcoxon signed-rank test demonstrated a statistically significant reduction in carbon black adhesion at the treated site (Z = −4.11, $p < 0.001$; 55.0% reduction relative to the untreated control site). The GEE model confirmed this between-group difference (SE = 4.82; 95% CI: −64.4 to −45.6; Wald Z = −11.41; $p < 0.001$; working correlation ρ = 0.63). Cohen's d = 2.43 (large effect). The group-level mean reduction rate was 55.0%. Results are presented in Table 2; representative skin images are shown in Figure 3.

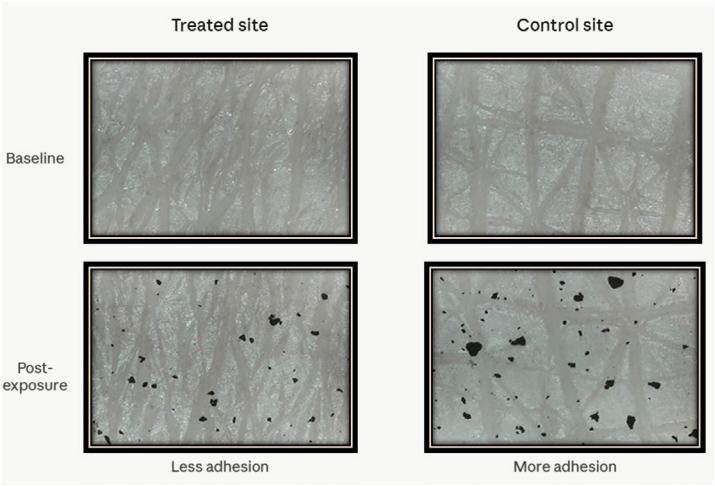


Figure 3. Representative digital microscope images of the skin surface before (baseline) and after carbon black exposure, shown as matched pairs from the same participant. Treated (**left**) and untreated control (**right**) sites are displayed side by side at each time point. Scale = 500 µm. Site labels ('Treated'/'Control') and participant code are shown on each panel; arrows indicate representative carbon black particle clusters. Images were selected from the same participant to ensure comparable skin microrelief between panels.

3.3. Consistency of Reduction Directionality Across Subjects

All 22 subjects (100%) showed lower pixel area in the treated site than in the control site, with no inverse responders. This indicates that the anti-adhesion effect was consistent across the cohort despite inter-individual variability in skin characteristics. CVs were nearly identical between groups (treated 52.4% vs. control 50.6%), indicating comparable relative variability. It should be noted that the group-level reduction rate in Table 2 (55.0%) was calculated from group means [(control mean − treated mean)/control mean × 100], whereas the mean individual reduction rate in Table 3 (51.8%) represents the arithmetic mean of subject-level reduction ratios; the modest discrepancy reflects the mathematical non-equivalence of ratio-based calculations performed at the group versus individual level. Under the null hypothesis, the probability of observing 100% directional consistency in 22 subjects by chance is $(0.5)^{22} < 0.001$ (exact binomial $p < 0.001$; sign test $Z = 4.47$, $p < 0.001$; Clopper–Pearson 95% CI for true responder proportion: 85.1–100.0%). Nevertheless, given $n = 22$, larger studies are needed to characterise potential non-responders.

3.4. Individual Reduction Rates and Robustness of Results

Individual reduction rates ranged from 22.62% (Subject No. 9) to 74.15% (Subject No. 21), with all 22 subjects showing positive values. The mean (51.8%) and median (52.3%) reduction rates were closely aligned, indicating a near-symmetric distribution without undue influence from extreme responders. Individual paired comparisons are presented in Table 3. Multiple sensitivity analyses confirmed robustness: (1) outlier-excluded analysis (±2 SD, no outliers identified): mean 51.8% (95% CI: 45.4–58.2%); (2) bootstrap (n = 10,000): mean 51.9% (bootstrap 95% CI: 45.4–58.2%); (3) Q1 subgroup (lowest quartile, $n = 5$): mean 30.1%—confirming meaningful reduction even among poorest responders. Full individual-level data in Supplementary Table S1.

Sensitivity analysis for Subject No. 14—who exhibited the highest absolute pixel values (treated: 12,994 pixels; control: 26,202 pixels; individual reduction rate: 50.41%)—produced an overall mean reduction rate of 51.9% after exclusion, consistent with the primary finding. This confirms that the observed efficacy was not driven by any single outlier.

Table 3. Summary of individual reduction rates and distribution metrics (n = 22).

Metric	Value
Subjects with positive reduction	22/22 (100%)
Mean reduction rate (%)	51.8
Median reduction rate (%)	52.3
SD of individual reduction rates (%)	15.8
IQR (Q1–Q3) (%)	39.3–67.1
SA1: Outlier exclusion (±2 SD)—mean (95% CI)	51.8% (45.4–58.2%)
SA2: Bootstrap mean (95% CI, 10,000 resamples)	51.9% (45.4–58.2%)
SA3: Excl. Subject 14—mean (%)	51.9
SA4: Q1 (lowest quartile, n = 5) mean (%)	30.2
SA4: Q4 (highest quartile, n = 5) mean (%)	69.9
Sign test: exact binomial p	<0.001 [$(0.5)^{22} = 2.4 \times 10^{-7}$]
Clopper–Pearson 95% CI for responder proportion	85.1–100.0%
Minimum reduction (%)	22.62 (Subject No. 9)
Maximum reduction (%)	74.15 (Subject No. 21)
CV, treated group (%)	52.4
CV, control group (%)	50.6

CV, coefficient of variation; SD, standard deviation; IQR, interquartile range; SA, sensitivity analysis; CI, confidence interval. Reduction rate = [(Control − Treated)/Control] × 100 per subject. SA1: $|Z| > 2.0$ excluded. SA2: bootstrap percentile (n = 10,000 resamples). See Supplementary Tables S1–S6 for full individual-level data.

4. Discussion

The present study validated a controlled in vivo test protocol using a patented exposure chamber to evaluate the anti-particulate adhesion efficacy of cosmetics, with platform validation as the primary objective. The 55.0% reduction in carbon black adhesion (Wilcoxon: Z = −4.11, $p < 0.001$; GEE: 95% CI −64.4 to −45.6; Cohen's d = 2.43), confirmed by four independent sensitivity analyses, demonstrates both the discriminative capacity of the chamber system and the anti-adhesion properties of the tested formulation.

The statistical significance of these results can be considered from three perspectives. First, $p < 0.001$ reflects a substantial effect size (approximately 55%), not merely an artefact of sample size. Second, the uniform reduction direction across all 22 subjects indicates that the anti-adhesion effect is consistent despite inter-individual differences in skin characteristics such as sebum secretion, surface roughness, and moisture content. Third, the sensitivity analysis—in which the reduction rate was virtually unchanged at 51.9% after exclusion of the extreme-value subject—demonstrates that the result is distributed evenly across the cohort and is not inflated by individual outliers. Together, these indicators support the reproducibility and reliability of the evaluation platform. The bootstrap 95% CI (45.4–58.2%) and outlier-excluded analyses (no ±2 SD outliers identified; primary mean 51.8%, 95% CI 45.4–58.2%) exclude the possibility that extreme responders drove the result. The exact binomial sign test ($p < 0.001$; Clopper–Pearson 95% CI 85.1–100.0%) provides formal statistical support for 100% directional consistency, whilst n = 22 limits definitive conclusions about population-level non-responder rates.

From a methodological perspective, the patented exposure chamber may offer potential advantages over conventional open-enclosure approaches [21–23]. Conventional open-enclosure systems rely on passive particle settling or manually directed spray without active environmental regulation, producing non-uniform particle distribution and

uncontrolled temperature and humidity that can introduce systematic bias between test and control sites. The present apparatus addresses these shortcomings through three integrated engineering features. First, the precision dual-stage pneumatic nozzle generates consistently sized aerosol droplets and drives particles uniformly throughout the chamber, eliminating concentration heterogeneity inherent in passive or single-stage systems. Second, the active air-circulation system maintains a dynamic particle environment that more faithfully replicates real-world atmospheric turbulence compared with static particle fields of sealed acrylic enclosures. Third, the automated post-test cleaning function—purging residual particles through a pre-filter, HEPA filter, and dust collector—returns the chamber to a particle-free baseline between runs, eliminating cross-contamination and safeguarding operator health. The Narda et al. [23] dermoscope-based carbon particle protocol—the closest published in vivo comparator—employed an open-enclosure application without concentration regulation. The Galliano et al. [25] forearm protocol, whilst validated for cleansing efficacy, did not use sealed-chamber exposure and cannot isolate PM deposition from ambient confounders. The accelerated exposure concentration (~100–1500× ambient PM_{10}) compresses real-world cumulative PM exposure into a 5 min session, consistent with established challenge paradigms [26,27]; translation to real-world conditions remains to be determined [7]. A direct head-to-head comparison with open-enclosure methods has not been performed; stated advantages rest on engineering principles and indirect evidence [22].

Several limitations should be acknowledged. First, the cohort was confined to females aged 46–68 years; sex differences could not be examined, and generalisability to males and younger age groups remains to be determined [27,34]. Second, the single-exposure design does not address long-term or cumulative efficacy. Third, evaluation was limited to carbon black; applicability to heterogeneous atmospheric PM, pollen, yellow dust, and PM2.5 requires further investigation [7,11,12]. Fourth, no direct head-to-head comparison with conventional open-enclosure approaches was performed; methodological advantages rest on engineering principles and indirect evidence. Fifth, pixel-based image analysis quantifies projected 2D surface coverage, not 3D particle mass; particles in follicular orifices may be undercounted, and the method cannot distinguish PM size subfractions (PM10 vs PM2.5 vs ultrafine). Sixth, CVs exceeding 50% reflect inter-individual variability in sebum production, surface microrelief, and hydration, which independently influence PM retention [15,30,31,35]; future studies should incorporate baseline topographic matching as a stratification variable. Seventh, the volar forearm differs from facial skin in sebum output, follicular density, and barrier function [27,34]; extrapolation to facial use should be made with caution. Eighth, the accelerated exposure concentration (~100–1500× ambient PM_{10}) was designed as a discriminative challenge paradigm; translation to real-world protection warrants further investigation [7,36].

5. Conclusions

The present study demonstrated that the patented particulate matter exposure chamber—incorporating a precision dual-stage spray nozzle, active internal particle circulation, and an automated HEPA-based cleaning system—provides a controlled, reproducible in vivo platform for anti-PM cosmetic efficacy evaluation. The primary finding—55.0% reduction in carbon black adhesion at the product-treated relative to the untreated site (Wilcoxon $Z = -4.11$, $p < 0.001$; GEE: 95% CI − 64.4 to −45.6; Cohen's d = 2.43; confirmed across four independent sensitivity analyses)—demonstrates the platform's discriminative capacity and the anti-adhesion properties of the tested formulation. This study should be understood as a proof-of-concept methodological validation rather than a product efficacy characterisation. The protocol provides a methodological foundation consistent with regu-

latory guidance for anti-PM claim substantiation [34]. Future studies should extend this protocol to multiple formulations, diverse particle types, repeated exposure paradigms, and cross-laboratory reproducibility assessments.

6. Patents

The anti-dust performance testing device used in this study is registered as Korean Patent No. 10-2020-0068941 (H.-J. Jeong, Human Skin Clinical Trial Center Co., Ltd., Seoul, Republic of Korea; filing date: 8 June 2020).

Supplementary Materials: The following supporting information can be downloaded at: https://www.mdpi.com/article/10.3390/cosmetics13030160/s1, Table S1: Individual-level carbon black adhesion data and reduction rates for all 22 subjects; Table S1a: Descriptive statistics for individual reduction rates (n = 22); Table S2: Full GEE parameter estimates and model specifications; Table S3: Bootstrap sensitivity analysis—distribution of mean individual reduction rate (n = 10,000 resamples); Table S4: Quartile subgroup analysis of individual reduction rates; Table S5: Outlier-exclusion sensitivity analyses; Table S6: Exact sign test and probability assessment for directional consistency.

Author Contributions: Conceptualisation, W.H. and H.K.; methodology, Y.K. (Youngrin Kwag); formal analysis, Y.K. (Youngrin Kwag); investigation, H.J. and Y.K. (Yoori Kang); data curation, H.J. and M.S.J.; writing—original draft preparation, Y.K. (Youngrin Kwag); writing—review and editing, W.H. and H.K.; visualisation, H.J.; resources, W.H.; supervision, W.H.; project administration, H.K. and Y.K. (Yoori Kang). All authors have read and agreed to the published version of the manuscript.

Funding: The clinical data presented in this study were derived from a human application trial funded by IALL Co., Ltd. (Seoul, Republic of Korea).

Institutional Review Board Statement: The study was conducted in accordance with the Declaration of Helsinki and approved by the Institutional Review Board of Human Skin Clinical Trial Center Co., Ltd. (protocol code HM-IRB-P25-1115; 17 December 2025).

Informed Consent Statement: Informed consent was obtained from all subjects involved in the study.

Data Availability Statement: The data presented in this study are available on request from the corresponding author. The data are not publicly available due to privacy restrictions.

Acknowledgments: The authors thank the research staff of Human Skin Clinical Trial Center Co., Ltd. for assistance with trial conduct and data management. During the preparation of this manuscript, the authors used Claude 4.6 (Anthropic, San Francisco, CA, USA) for language editing. The authors have reviewed and edited the output and take full responsibility for the content of this publication.

Conflicts of Interest: Won-Kyu Hong and Hong Seok Kim are directors of Class one Clinic and VOS Dermatology Clinic, respectively. Y.K., H.J., Y.-R.K., and M.S.J. are employees of Human Skin Clinical Trial Center Co., Ltd. H.J., as the representative of Human Skin Clinical Trial Center Co., Ltd., holds intellectual property rights to the particulate exposure chamber used in this study (Korean Patent No. 10-2020-0068941). The remaining authors declare that the research was conducted in the absence of any commercial or financial relationships that could be construed as a potential conflict of interest. The test product was provided by a commercial entity (IALL Co., Ltd.); however, the sponsors had no role in the design of the present study; in the analysis or interpretation of data; in the writing of the manuscript; or in the decision to publish the results.

Abbreviations

PM	Particulate matter
ROS	Reactive oxygen species
GEE	Generalised estimating equation (complementary between-group analysis)
HEPA	High-efficiency particulate air
IRB	Institutional Review Board

CV	Coefficient of variation
SD	Standard deviation
INCI	International Nomenclature of Cosmetic Ingredients
ROI	Region of interest
TEWL	Transepidermal water loss
AhR	Aryl hydrocarbon receptor
IQR	Interquartile range
CI	Confidence interval
ICP-MS	Inductively coupled plasma mass spectrometry
SA	Sensitivity analysis

References

1. Drakaki, E.; Dessinioti, C.; Antoniou, C.V. Air pollution and the skin. *Front. Environ. Sci.* **2014**, *2*, 11. [CrossRef]
2. Krutmann, J.; Liu, W.; Li, L.; Pan, X.; Crawford, M.; Sore, G.; Seite, S. Pollution and skin: From epidemiological and mechanistic studies to clinical implications. *J. Dermatol. Sci.* **2014**, *76*, 163–168. [CrossRef] [PubMed]
3. Magnani, N.D.; Muresan, X.M.; Belmonte, G.; Cervellati, F.; Sticozzi, C.; Pecorelli, A.; Miracco, C.; Marchini, T.; Evelson, P.; Valacchi, G. Skin damage mechanisms related to airborne particulate matter exposure. *Toxicol. Sci.* **2016**, *149*, 227–236. [CrossRef] [PubMed]
4. Kim, K.E.; Cho, D.; Park, H.J. Air pollution and skin diseases: Adverse effects of airborne particulate matter on various skin diseases. *Life Sci.* **2016**, *152*, 126–134. [CrossRef] [PubMed]
5. Araviiskaia, E.; Berardesca, E.; Bieber, T.; Gontijo, G.; Sanchez Viera, M.; Marrot, L.; Chuberre, B.; Dreno, B. The impact of airborne pollution on skin. *J. Eur. Acad. Dermatol. Venereol.* **2019**, *33*, 1496–1505. [CrossRef] [PubMed]
6. Lee, C.W.; Lin, Z.C.; Hu, S.C.; Chiang, Y.C.; Hsu, L.F.; Lin, Y.C.; Lee, I.T.; Tsai, M.H.; Fang, J.Y. Urban particulate matter down-regulates filaggrin via COX2 expression/PGE2 production leading to skin barrier dysfunction. *Sci. Rep.* **2016**, *6*, 27995. [CrossRef] [PubMed]
7. Marrot, L. Pollution and sun exposure: A deleterious synergy. Mechanisms and opportunities for skin protection. *Curr. Med. Chem.* **2018**, *25*, 5469–5486. [CrossRef] [PubMed]
8. Pecorelli, A.; Woodby, B.; Prieux, R.; Valacchi, G. Involvement of 4-hydroxy-2-nonenal in pollution-induced skin damage. *Biofactors* **2019**, *45*, 536–547. [CrossRef] [PubMed]
9. Vierkötter, A.; Schikowski, T.; Ranft, U.; Sugiri, D.; Matsui, M.; Krämer, U.; Krutmann, J. Airborne particle exposure and extrinsic skin aging. *J. Investig. Dermatol.* **2010**, *130*, 2719–2726. [CrossRef] [PubMed]
10. Hyun, Y.J.; Piao, M.J.; Kang, K.A.; Zhen, A.X.; Madushan Fernando, P.D.S.; Kang, H.K.; Ahn, Y.S.; Hyun, J.W. Effect of fermented fish oil on fine particulate matter-induced skin aging. *Mar. Drugs* **2019**, *17*, 61. [CrossRef] [PubMed]
11. Park, S.Y.; Byun, E.J.; Lee, J.D.; Kim, S.; Kim, H.S. Air pollution, autophagy, and skin aging: Impact of particulate matter (PM10) on human dermal fibroblasts. *Int. J. Mol. Sci.* **2018**, *19*, 2727. [CrossRef] [PubMed]
12. Piao, M.J.; Ahn, M.J.; Kang, K.A.; Ryu, Y.S.; Hyun, Y.J.; Shilnikova, K.; Zhen, A.X.; Jeong, J.W.; Choi, Y.H.; Kang, H.K.; et al. Particulate matter 2.5 damages skin cells by inducing oxidative stress, subcellular organelle dysfunction, and apoptosis. *Arch. Toxicol.* **2018**, *92*, 2077–2091. [CrossRef] [PubMed]
13. Jin, S.P.; Li, Z.; Choi, E.K.; Lee, S.; Kim, Y.K.; Seo, E.Y.; Chung, J.H.; Cho, S. Urban particulate matter in air pollution penetrates into the barrier-disrupted skin and produces ROS-dependent cutaneous inflammatory response in vivo. *J. Dermatol. Sci.* **2018**, *91*, 175–183. [CrossRef] [PubMed]
14. Boo, Y.C. Can plant phenolic compounds protect the skin from airborne particulate matter? *Antioxidants* **2019**, *8*, 379. [CrossRef] [PubMed]
15. Mistry, N. Guidelines for formulating anti-pollution products. *Cosmetics* **2017**, *4*, 57. [CrossRef]
16. Lee, J.; Oh, S.J.; Park, S.; Park, J.H.; Lee, J.H. Anti-pollution skincare: Research on effective ways to protect skin from particulate matter. *Dermatol. Ther.* **2021**, *34*, e14960. [CrossRef] [PubMed]
17. Hüls, A.; Vierkötter, A.; Gao, W.; Krämer, U.; Yang, Y.; Ding, A.; Stolz, S.; Matsui, M.; Kan, H.; Wang, S.; et al. Traffic-related air pollution contributes to development of facial lentigines: Further epidemiological evidence from Caucasians and Asians. *J. Investig. Dermatol.* **2016**, *136*, 1053–1056. [CrossRef] [PubMed]
18. Lefebvre, M.A.; Pham, D.M.; Boussouira, B.; Bernard, D.; Camus, C.; Nguyen, Q.L. Evaluation of the impact of urban pollution on the quality of skin: A multicentre study in Mexico. *Int. J. Cosmet. Sci.* **2015**, *37*, 329–338. [CrossRef] [PubMed]
19. Dijkhoff, I.M.; Drasler, B.; Karakocak, B.B.; Petri-Fink, A.; Valacchi, G.; Eeman, M.; Rothen-Rutishauser, B. Impact of airborne particulate matter on skin: A systematic review from epidemiology to in vitro studies. *Part. Fibre Toxicol.* **2020**, *17*, 35. [CrossRef] [PubMed]

20. Iwanaga, T.; Nioh, A.; Reed, N.; Kiyokawa, H.; Akatsuka, H. A novel water-in-oil emulsion with a lecithin-modified bentonite prevents skin damage from urban dust and cedar pollen. *Int. J. Cosmet. Sci.* **2020**, *42*, 229–236. [CrossRef] [PubMed]
21. Narda, M.; Bauza, G.; Valderas, P.; Granger, C. Protective effects of a novel facial cream against environmental pollution: In vivo and in vitro assessment. *Clin. Cosmet. Investig. Dermatol.* **2018**, *11*, 571–578. [CrossRef] [PubMed]
22. Curpen, S.; Francois-Newton, V.; Moga, A.; Hosenally, M.; Petkar, G.; Soobramaney, V.; Ruchaia, B.; Lutchmanen Kolanthan, V.; Roheemun, N.; Sokeechand, B.N.; et al. A novel method for evaluating the effect of pollution on the human skin under controlled conditions. *Skin Res. Technol.* **2020**, *26*, 50–60. [CrossRef] [PubMed]
23. Kim, S.; Kim, S.; Shon, D.; Kim, A.R.; Kim, H.J.; Kim, E. Equivalence of in vitro and in vivo methods for assessing the effectiveness of anti-particulate matter pollution products. *Skin Res. Technol.* **2021**, *27*, 49–55. [CrossRef] [PubMed]
24. Pandis, N. Sample calculation for split-mouth designs. *Am. J. Orthod. Dentofac. Orthop.* **2012**, *141*, 818–819. [CrossRef] [PubMed]
25. Hanley, J.A.; Negassa, A.; Edwardes, M.D.; Forrester, J.E. Statistical analysis of correlated data using generalized estimating equations: An orientation. *Am. J. Epidemiol.* **2003**, *157*, 364–375. [CrossRef] [PubMed]
26. Liang, K.Y.; Zeger, S.L. Longitudinal data analysis using generalized linear models. *Biometrika* **1986**, *73*, 13–22. [CrossRef]
27. Firooz, A.; Sadr, B.; Babakoohi, S.; Sarraf-Yazdy, M.; Fanian, F.; Kazerouni-Timsar, A.; Nassiri-Kashani, M.; Naghizadeh, M.M.; Dowlati, Y. Variation of biophysical parameters of the skin with age, gender, and body region. *Sci. World J.* **2012**, *2012*, 386936. [CrossRef] [PubMed]
28. Ministry of Food and Drug Safety (MFDS). Chapter 10: Anti-Particulate Matter Adhesion Blocking Test. In *Guideline for Test Methods to Substantiate Cosmetic Claims*; MFDS: Cheongju, Republic of Korea, 2018. Available online: https://www.mfds.go.kr/brd/m_1060/view.do?seq=15567 (accessed on 30 April 2026).
29. Rembiesa, J.; Ruzgas, T.; Engblom, J.; Holefors, A. The impact of pollution on skin and proper efficacy testing for anti-pollution claims. *Cosmetics* **2018**, *5*, 4. [CrossRef]
30. Paik, K.; Na, J.-I.; Huh, C.-H.; Shin, J.-W. Particulate matter and its molecular effects on skin: Implications for various skin diseases. *Int. J. Mol. Sci.* **2024**, *25*, 9888. [CrossRef] [PubMed]
31. Boonpethkaew, S.; Charoensuksira, S.; Meephansan, J.; Sirithanabadeekul, P.; Chueachavalit, C.; Ingkaninanda, P.; Visedthorn, S.; Chanchaem, P.; Sivapornnukul, P.; Payungporn, S. The influence of air pollution on skin microbiome: A link to skin barrier dysfunction. *Arch. Dermatol. Res.* **2024**, *316*, 710. [CrossRef] [PubMed]
32. Dähnhardt, D.; Dähnhardt-Pfeiffer, S.; Simon, I.; Ditgen, D.; Holland, I.; Segger, D.; Blaak, J.; Staib, P. Protective and Regenerative Anti-Pollution Efficacy of a Plant Oil-Based Day and Night Cream: Investigated by a Novel Approach to Reveal the Impact of Pollutants on Epidermal Barrier Integrity and Lipid Matrix. *J. Cosmet. Dermatol. Sci. Appl.* **2023**, *13*, 285–304. [CrossRef]
33. Galliano, A.; Ye, C.; Su, F.; Wang, C.; Rakshit, R.; Guerin, M.; Flament, F.; Steel, A. Assessing the effect of cleansing products on artificially polluted human hairs and skin through in vivo and in vitro models. *Skin Res. Technol.* **2023**, *29*, e13220. [CrossRef] [PubMed]
34. Gorcea, M.; Lane, M.E.; Moore, D.J. A proof-of-principle study comparing barrier function and cell morphology in face and body skin. *Int. J. Cosmet. Sci.* **2019**, *41*, 613–616. [CrossRef] [PubMed]
35. Oh, S.J.; Yoon, D.; Park, J.-H.; Lee, J.H. Effects of Particulate Matter on Healthy Skin: A Comparative Study between High- and Low-Particulate Matter Periods. *Ann. Dermatol.* **2021**, *33*, 263–270. [CrossRef] [PubMed]
36. Lange, K.M.; Sullivan, T.R.; Kasza, J.; Yelland, L.N. Performance of mixed effects models and generalized estimating equations for continuous outcomes in partially clustered trials including both independent and paired data. *Stat. Med.* **2024**, *43*, 4819–4835. [CrossRef] [PubMed]

Disclaimer/Publisher's Note: The statements, opinions and data contained in all publications are solely those of the individual author(s) and contributor(s) and not of MDPI and/or the editor(s). MDPI and/or the editor(s) disclaim responsibility for any injury to people or property resulting from any ideas, methods, instructions or products referred to in the content.